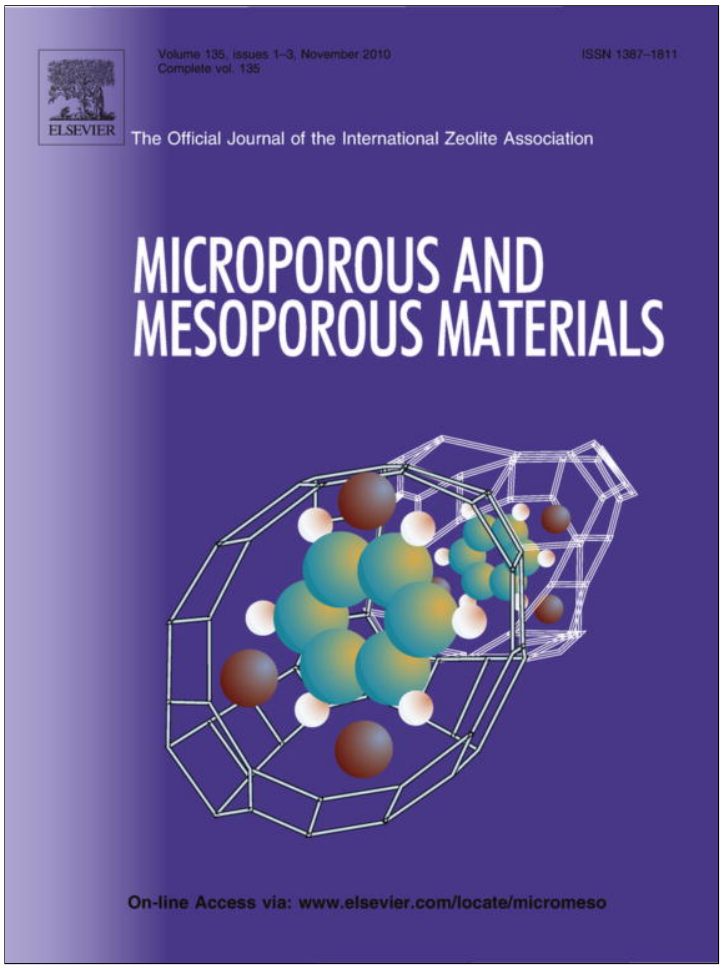

Microporous and Mesoporous Materials 135 (2010) 161–169

Contents lists available at ScienceDirect

Microporous and Mesoporous Materials

journal homepage: www.elsevier.com/locate/micromeso

Thin films of cubic mesoporous aluminophosphates modified by silicon and manganese

Saša Cecowski [a], Nataša Novak Tušar [a,*], Mojca Rangus [a], Gregor Mali [a], Galo J.A.A. Soler-Illia [b], Venčeslav Kaučič [a]

[a] Laboratory for Inorganic Chemistry and Technology, National Institute of Chemistry, Hajdrihova 19, 1000 Ljubljana, Slovenia
[b] Gerencia de Quimica, Comisión Nacional de Energía Atómica, Av. Gral Paz 1499 B1650KNA, San Martín, Buenos Aires, Argentina;CONICET, Av. Rivadavia 1917, C1033AAV, Buenos Aires, Argentina

ARTICLE INFO

Article history:
Received 22 February 2010
Received in revised form 30 June 2010
Accepted 6 July 2010
Available online 3 August 2010

Keywords:
Thin films
Silicon and manganese modified cubic mesoporous aluminophosphate
AFM
NMR
EXAFS

ABSTRACT

Mesoporous aluminophosphate thin films and xerogels with ordered three-dimensional pore arrangement, modified by silicon or silicon and manganese, were synthesized. Aluminophosphate reaction mixtures were templated with non ionic polymer surfactant Pluronic F127 and deposited as thin layers of precursor solution on Petri dishes for xerogels and on glass substrates for thin films. Surfactant removal was investigated by thermal analysis. Small Angle X-ray Scattering measurements showed that calcined silicoaluminophosphate (SAPO) and manganese silicoaluminophosphate (MnSAPO) thin films have highly ordered mesostructures, which remain stable up to at least 400 °C. The mesostructures exhibit cubic symmetry described by an $Im\bar{3}m$ space group. Cubic mesostructure was confirmed also by TEM, SEM and AFM microscopy. Incorporation of silicon and manganese into the aluminophosphate framework was studied by solid-state NMR and X-ray absorption spectroscopy. Silicon-rich domains were detected in calcined SAPO and MnSAPO xerogels and in MnSAPO thin films. The observation of $Si(OSi)_3(OAl)$ framework units at the border of such domains suggests that acid sites might be included within silicoaluminophosphate walls. Mn^{3+} and Mn^{2+} cations are present in the MnSAPO frameworks of calcined xerogels and thin films in the molar ratio of 40%/60%. Manganese cations are coordinated to four oxygen atoms, suggesting that they are incorporated within the framework and that they can act as framework redox sites.

1. Introduction

After the discovery of mesoporous silicate MCM-41 by Mobil scientists in 1992 [1,2] a series of mesostructured and mesoporous materials with diverse chemical compositions were prepared in the form of powders, monoliths, thin films, membranes and fibers for various catalytic applications [3]. The first publications on mesoporous materials with aluminophosphate composition appeared in 1993. They presented lamellar structures, which were not thermally stable [4]. During the following 15 years a lot of effort was devoted to the synthesis of mesostructured aluminophosphates by supramolecular structure direction [5]. The research, summarized in two review papers [6,7], lead to a large variety of synthetic approaches and yielded materials with various structural properties. Researchers were also focused on developing novel strategies for synthesis of metal-modified aluminophosphates and for incorporating these new materials into emerging applications in the fields of separations, catalysis, sensing, optics and host–guest assemblies [8]. In the particular case of aluminophosphate frameworks, applications are sought in which the catalytic properties can be exploited in the case of bulkier molecules [9]. It is also important to tune the acidity of the surface sites by the controlled incorporation of Si or other metals in the AlPO framework, therefore introducing a charge unbalance. The intimate incorporation of these heteroatom sites within the frameworks is a requisite for the formation of both Lewis and Brønsted sites, which lead to a variety of applications [10]. The possibility of producing supramolecularly templated substituted AlPO materials provide large-pore strong solid acid matrices with tunable proton mobility [5]. Mesoporous AlPO or SAPO matrices can lead to higher acidity than the microporous analogues and a higher amount of strong acid sites, which is tunable with the silicon content [11]. In addition, high catalytic activity and selectivity are obtained in several reactions such as Beckmann rearrangement [12]. Substitution with transition metal ions such as Mn present potential interest in selective partial oxidation [13] or the skeletal isomerization of *n*-butenes [14].

* Corresponding author. Tel.: +386 1 4760310; fax: +386 1 4760300.
E-mail address: natasa.novak@ki.si (N.N. Tušar).

1387-1811/$ - see front matter © 2010 Elsevier Inc. All rights reserved.
doi:10.1016/j.micromeso.2010.07.005

Thus far the majority of studies dealt with periodically organized mesoporous materials in the form of powders. In comparison to powdered materials, periodically organized mesoporous thin films present two major advantages: (i) modification and functionalization of the framework of thin films is easier due to easier pore accessibility (ii) thin films enable miniaturization of devices (iii) the materials can be easily and reproducibly deposited onto a variety of substrates, including catalyst supports. A recent review on the design, synthesis and properties of thin films exhibiting periodically organized nanopores contains a more extensive discussion on major advances [15].

Recently Mazaj et al. [16] have developed cubic 3D mesoporous aluminophosphate thin films by evaporation-induced self-assembly (EISA) using two different non ionic polymer surfactants, Pluronic F127 and F108. As explained, the formation mechanism of these AlPO phases is similar to the mechanism observed for transition metal oxides and can be summarized in the following steps [17,18]:

1. Small hydrophilic cluster-like nanobuilding blocks (NBB) are formed in the initial solutions.
2. The clusters coassemble with template micelles or liquid crystalline mesophases upon evaporation; the fact that NBB are hydrophilic directs them to interact with the hydrophilic block of the template molecule.
3. An initial locally ordered mesophase forms and evolves to a highly ordered mesophase provided that the initially formed template-NBB-solvent gel is mobile enough to permit rearrangements.
4. The mesostructure is "locked" upon thermal treatment.

In this work, we report on the preparation and structural characterization of aluminophosphate (AlPO) mesoporous xerogels and thin films with 3D pore arrangement modified by silicon (SAPO) and manganese (MnSAPO). We decided for modification of the framework with silicon, because the incorporation of silicon into microporous aluminophosphate frameworks already proved to yield materials with higher surface areas and better thermal stability [19]. Incorporation of manganese into microporous and mesoporous aluminophosphate frameworks is known to result in materials with catalytic functions [7,20,21]. Such catalysts are nowadays interesting because of manganese non-toxic and cost-effective nature, and even more because of its wide range of oxidation states (2+ to 7+).

2. Experimental

2.1. Preparation of mesostructured materials

Mesoporous xerogels and thin films were prepared by evaporation-induced self-assembly under controlled temperature and relative humidity, using a modified procedure of the one described in Ref. [16]. Initial sol was prepared by mixing $AlCl_3 * 6H_2O$ (99% Sigma Aldrich), tetraethil orthosilicate (98% TEOS, Acros Organics) and manganese acetate ($Mn(CH_3COO) * 4H_2O$, Aldrich) with ethanol (EtOH absolute, Sigma–Aldrich) prior to the addition of phosphoric acid (85% H_3PO_4, Merck). Pure SAPO was prepared without manganese acetate. The solution was stirred for 2 h and subsequently block copolymer Pluronic F127 (Sigma–Aldrich) was added under stirring. Clear solution, with molar ratio $1AlCl_3 * 6H_2O$:$1H_3PO_4$:0.2-TEOS:0005F127:50EtOH:(0.01–0.05)$Mn(CH_3COO) * 4H_2O$, was obtained after 2 h of stirring. Thin films were deposited on clean glass substrate and silicon wafers (100, Aldrich) by dip-coating at a constant withdrawal speed of 2 mm/s at ambient (295–300 K) temperature and relative humidity of 40–50%. The relative humidity was controlled by performing dip-coating in a closed chamber with a controlled relative humidity atmosphere. As prepared films were aged at ambient temperature and relative humidity of 40–50% for 24 h, at 60 °C for 24 h, at 130 °C for 24 h. The three different aging steps for thin films at three different temperatures are necessary in order to optimize the formation of a highly ordered mesophase [25b]. Finally the films were calcined at 400 °C for 6 h.

SAPO xerogels were produced by transferring the precursor solution into Petri dishes, where ethanol evaporated at humidity between 40% and 50% and at ambient temperature. Afterwards the product was dried at 60 °C for 1 day, at 80 °C for 2 h and finally the obtained powder was calcined at 400 °C for 6 h.

2.2. Characterization methods

To investigate long-range structural properties of the obtained mesostructures, 2D SAXS experiments at incidence angles of 3° and 90° were performed at the D11A-SAXS1 line in the Laboratório Nacional de Luz Sincrotron (LNLS), Campinas, SP, Brazil, using $\lambda = 1.488$ Å and a sample-detector distance of 669.5 mm; image plates were used as detectors. Thickness and surface porosity of calcined films were determined by scanning electron microscopy (SEM) on a Zeiss Supra 3VP SEM microscope. Line scan elemental analysis was performed by energy dispersive X-ray spectroscopy (EDX) using an INCA Energy system attached to the same microscope. Transmission electron microscopy (TEM) was carried out on a 200-kV field-emission gun (FEG) microscope JEOL JEM 2100. The sample that was used for TEM study was a film scratched from a substrate and placed, with a drop of ethanol, on a copper holey carbon grid. The grid with the sample was left at room temperature to dry completely. Thermogravimetric analysis (TG-DTG) was performed on SDT 2960 thermal analysis system (TA Instruments, Inc.). The measurement was made on the thin film sample scratched from the glass substrate and on the xerogel that was prepared in a Petri dish. It was carried out in static air with a heating rate of 10 °C/min from room temperature to 600 °C.

An Agilent 5500 atomic force microscope (AFM) was used for the topographic characterization of the calcined SAPO and MnSAPO thin films on a glass substrate. NCHR-SuperSharpSilicon probes made by NanoSensors with a tip curvature radius of 2 nm, 330 kHz resonance frequency, and a spring constant of 42 N/m were used. The imaging was performed in non-contact mode (NC-mode), at room humidity and temperature. The average scan size was 1 μm × 1 μm. Scans were made with scan rate of 1.4 lines/s and with 512 line resolution.

^{31}P, ^{27}Al and ^{29}Si MAS NMR spectra of SAPO xerogels and of samples scratched from films were recorded on 600 MHz Varian NMR system equipped with a Varian 3.2 mm MAS probe. Fifty-five two-faced films (25 synthesized and 30 calcined) deposited on glass slides were needed to obtain sufficient amount of material for NMR measurements. Larmor frequencies for phosphorus, aluminium and silicon at 14.1 T are 242.89, 156.35 and 119.15 MHz, respectively. Chemical shifts are reported relative to the signal of ^{31}P in 85% H_3PO_4, ^{27}Al in 1 M solution of $Al(NO_3)_3$ and ^{29}Si in tetramethylsilane. To enhance the sensitivity of ^{29}Si signal, 'Carr–Purcell–Meiboom–Gill (CPMG) detection' was employed [22]. Samples of SAPO were in all experiments spun at 10 kHz, while samples of MnSAPO were spun at frequencies of up to 20 kHz.

X-ray absorption spectra of MnSAPO samples and reference compounds (Mn metal, $Mn^{2+}O$, Mn_3O_4, $K_3[Mn^{3+}(C_2O_4)_3] * 3H_2O$ and $Mn^{4+}O_2$) were measured in the energy region of the Mn K-edge in transmission and fluorescence detection mode at C beam line of HASYLAB synchrotron facility at DESY in Hamburg. A Si(1 1 1) double crystal monochromator was used with about 1.5 eV resolution at the Mn K-edge. Harmonics were effectively

eliminated by a slight detuning of the second monochromator crystal, keeping the intensity at 60% of the rocking curve with the beam stabilization feedback control. The intensity of the monochromatic X-ray beam was measured by three consecutive ionization chambers. The xerogel samples were prepared as self-supporting pellets with absorption thickness (μd) of about 2.5 above the Mn K-edge. The reference compounds, in the form of fine powders, were mixed with boron nitride powder to obtain self standing pellets with a total absorption thickness of 1.5 above the Mn K-edge. For the thin films samples, the fluorescence detection mode was used, exploiting a seven-element Si(Li) fluorescence detector. The absorption spectra were obtained as the ratio of the fluorescence detector signal and the signal of the incident photon beam from the first ionization chamber. The pellets were mounted on a sample holder in a vacuum chamber of the beam line, so that they were kept in high vacuum during measurements. The absorption spectra were measured within the interval [−250 eV, −1000 eV] relative to the Mn K-edge. In the XANES region equidistant energy steps of 0.5 eV were employed, while for the EXAFS region equidistant k-steps ($\Delta k \approx 0.03$ Å^{-1}) were adopted with the integration time of 2 s/step. Six repetitions were collected for each sample and superimposed to improve signal-to-noise ratio. Exact energy calibration was established with the simultaneous absorption measurements on Mn metal foil inserted between the second and third ionization cell. The quantitative analysis of Mn K-edge EXAFS spectra was performed with the IFEFFIT program packages [23] using FEFF6 code [24], in which the photoelectron scattering paths were calculated ab initio from a presumed distribution of neighboring atoms. Fourier transforms of k^3-weighted Mn EXAFS spectra were calculated in the k range of 3.4 and 3.4–11.5 Å^{-1} for as-synthesized and calcined MnSAPO thin films, respectively.

3. Results and discussion

3.1. Structure characterization

Structural characteristics of mesostructured SAPO and MnSAPO thin films, thermally treated at 400 °C, were investigated by SAXS (Fig. 1). The well-defined scattering patterns showed that the mesostructure presents a distorted structure derived from a body centered cubic symmetry (space group $Im\bar{3}m$) with [1 1 0] planes oriented parallel to the substrate [25]. Upon thermal treatment this cubic mesostructure is uniaxially compressed along the z axis; the resulting distorted unit cell can be more appropriately described by a face centered orthorhombic symmetry $Fmmm$ with the [0 1 0] plane oriented parallel to the surface, as described by Hillhouse and coworkers [26]. However, it is more customary to report the a lattice parameter of the original cubic mesophase, as well as the distortion of that parameter along the z axis. These data can both be extracted from SAXS patterns.

In all analyzed samples, SAPO and MnSAPO thin films exhibited a parameters of 19.5 ± 0.3 nm, and a contraction of 51–55% for samples calcined at 400 °C. These parameters are in good agreement with those found in cubic-derived F127-templated mesoporous silica and AlPO [16]. No significant differences were found between samples with varying Mn content, suggesting that the effect of metal inclusion in the material is too small to modify the mesostructure behavior. For further characterization we used SAPO xerogel and thin film with aluminium-to-manganese ratio of 20.

TEM micrographs of SAPO thin film in Fig. 2 reveal highly ordered large pore mesostructure after calcination, indicating thermally stable mesostructure. The estimated distance between the channels running along the (1 1 0) direction is 14.5 nm, which is in good agreement with SAXS measurements (d_{110} = 14 nm). Smooth and continuous surfaces of calcined SAPO and MnSAPO thin films were observed by FEG–SEM (Fig. 3). From the cross section of FEG–SEM images film thickness of 250 nm was estimated. Images in Fig. 3 also show surfaces of calcined SAPO and MnSAPO thin films, where the pores are clearly seen. With FFT filtering of these images highly ordered mesoporous cubic structure in (1 1 0) direction is confirmed.

Morphology of the thin film surface was further investigated by atomic force microscopy (Fig. 4). AFM provides information on surface roughness, pore dimensions and on the lattice parameter parallel to the film substrate. Calcined SAPO and MnSAPO thin films exhibit low surface roughness. Ordering of mesopores can be seen in AFM images of both films. Pore diameters in both samples were estimated to approximately 10 nm. Two-dimensional FFT performed on a selected zone of the AFM image of SAPO thin film (Fig. 4a) exhibits a "4 + 2" pattern, with four spots at shorter, and two at longer distances. The short-to-long-distance ratio is 0.85, which compares well with the theoretical value of 0.866 and which is typical for a [1 1 0] oriented body centered cubic mesophase [27]. The distances in the reciprocal space are related to pore-to-pore distances in the direct space. In SAPO thin film pore-to-pore distances along the [1 1 0] direction were estimated to be 14.5 nm, which is in good agreement with TEM and SAXS measurements reported above.

2D FFT was performed also on a selected part of AFM micrograph of the MnSAPO film (Fig. 4b). The obtained pattern of six spots equally distant from the center corresponds to [1 1 1] surface of the mesostructure with an $Im\bar{3}m$ symmetry. Pore-to-pore distance in the studied direction was estimated to 15 nm. FFT performed on other sections of AFM images revealed that MnSAPO thin films exhibit mesoporous structure that is not as highly ordered as it is in SAPO films and that different pore directions parallel to the substrate are possible. It seems that the addition

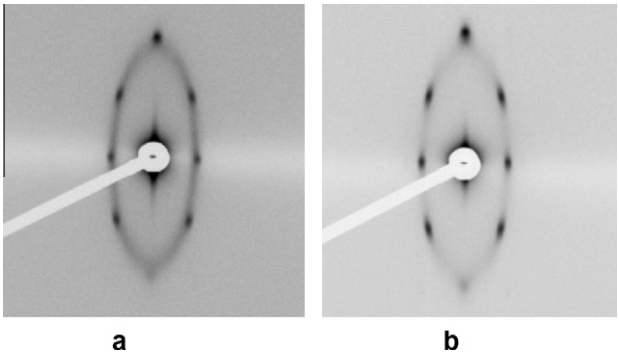

Fig. 1. SAXS patterns of calcined SAPO thin film (a) and MnSAPO thin film (b).

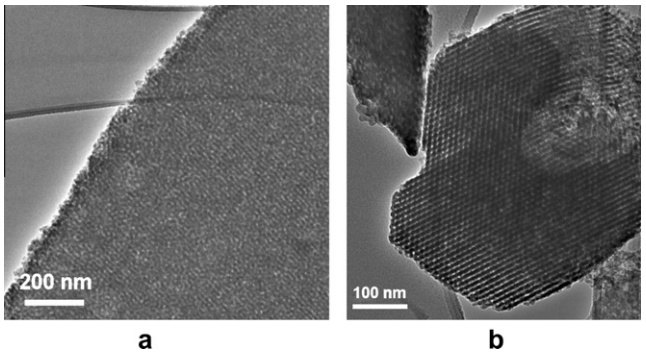

Fig. 2. TEM images of calcined SAPO thin films along (a) (1 1 0) and (b) (1 11) directions.

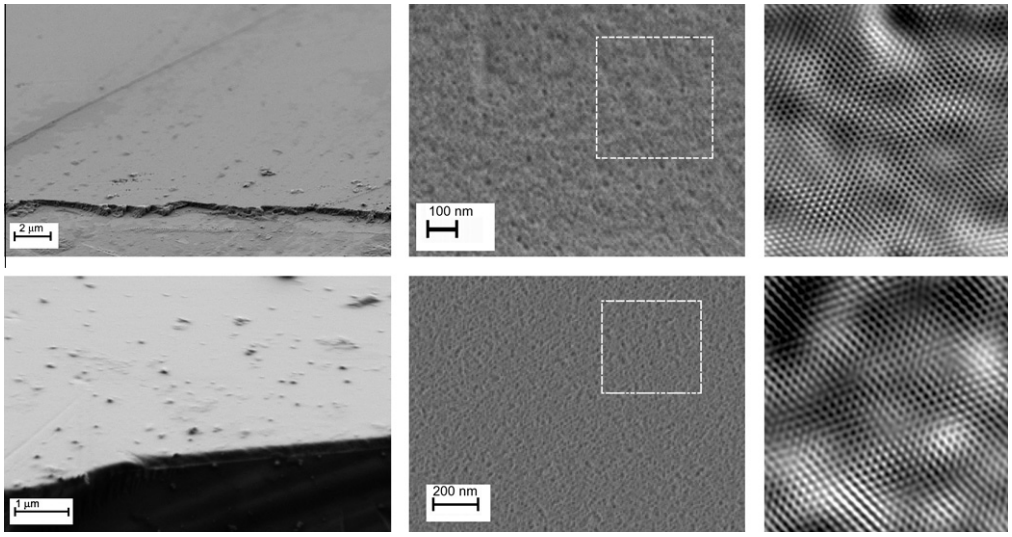

Fig. 3. FEG–SEM images of calcined SAPO thin film (upper row) and calcined MnSAPO thin film (lower row) show smooth and continuous surface (a), highly ordered mesoporous cubic structure in (1 1 0) direction (b), and FFT-filtered image of the corresponding micrograph from the selected area in figure b (c).

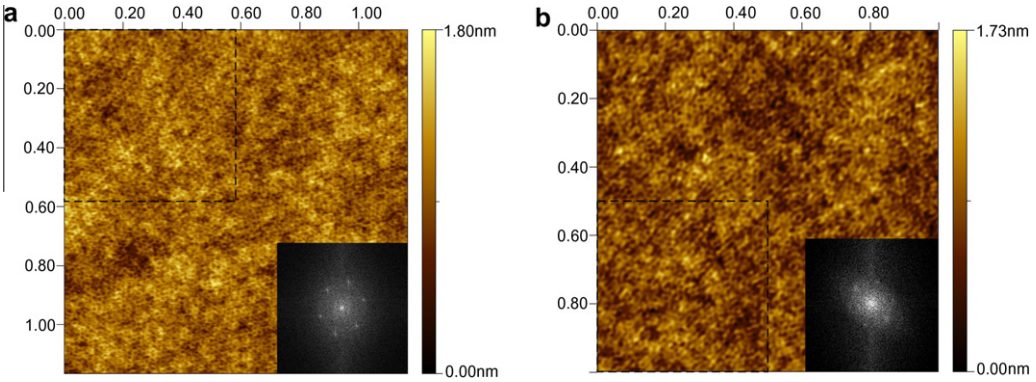

Fig. 4. AFM images of calcined SAPO (a) and MnSAPO (b) films on glass substrates. In insets there are 2D Fourier transforms of sections marked by dotted lines.

of manganese to the initial sol results in formation of smaller domains. In different domains mesopores are oriented in different directions in the *xy* plane. Such mosaic patterns were already detected in similar systems[25a,b].

Thermogravimetric analyses of mesoporous SAPO and MnSAPO thin films and xerogels (TG and DTG curves are shown in Fig. 5) indicate a total weight loss of about 50 wt.% up to 600 °C for thin films and xerogels. The inclusion of manganese into silicoaluminophosphate does not induce a significant change in the TG or DTG curve, neither for xerogels nor for thin films.

The first weight loss of 15–20 wt.% up to 150 °C for thin films and up to 180 °C for xerogels is attributed to water and ethanol desorption. The second weight loss of 25–30 wt.% is assigned to the removal of block copolymer species from the pores by decomposition or oxidation and desorption of its fragments. The results are in good agreement with F127-templated pure aluminophosphate thin films described in Ref. [16].

3.2. Incorporation of Si and Mn into thin films and xerogels

Formation of SAPO and MnSAPO thin films and xerogels, and local environment of incorporated silicon was investigated by solid-state NMR spectroscopy. ^{27}Al MAS NMR spectra of mesoporous SAPO thin films are very similar to NMR spectra obtained on the related cubic mesoporous AlPO thin films [9,21]. In the as-prepared SAPO film nearly all aluminium atoms are hexa-coordinated. After calcination, part of aluminium transforms to tetra- (30%) or penta-coordinated species (10%). ^{31}P MAS NMR spectra exhibit relatively broad signals with maxima between −10 and −20 ppm, suggesting that the SAPO framework is not fully condensed, neither in the as-prepared film nor in the calcined film. Moreover, the contribution of the phosphorus component with chemical shift of about −10 ppm, which can be assigned to phosphorus nuclei with less than four aluminium atoms in the first cation coordination sphere, is more pronounced in the calcined film than in the as-prepared one. This is surprising, because thermal treatment usually enhances the degree of condensation of the framework and thus increases the fraction of $P(OAl)_4$ groups and decreases the fractions of $P(OAl)_3OH$ and $P(OAl)_2(OH)_2$ groups. It seems that framework of SAPO thin film is quite sensitive to the removal of template molecules.

As already observed in case of the cubic mesoporous AlPO, condensation in xerogels proceeds differently than in films [16]. Fig. 6 shows ^{27}Al and ^{31}P MAS NMR spectra of the as-prepared and calcined SAPO xerogels. One can see that the as-prepared material already contains a substantial fraction of tetra-coordinated aluminium, and that in the calcined material only traces of hexa- and penta-coordinated aluminium remain. After calcination ^{31}P NMR signal becomes narrower and shifts to −27 ppm, suggesting that most of phosphorus atoms belong to $P(OAl)_4$ groups. It seems

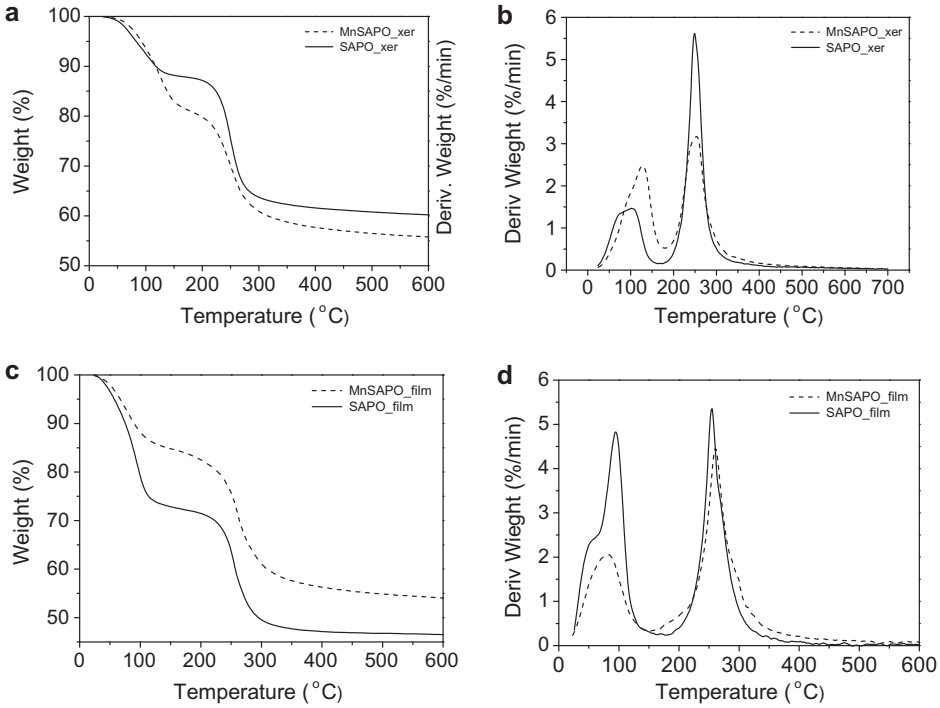

Fig. 5. TG (a) and DTG (b) curves of SAPO and MnSAPO xerogels, both treated at 60 °C. TG (c) and DTG (d) curves of SAPO and MnSAPO thin films, also both treated at 60 °C.

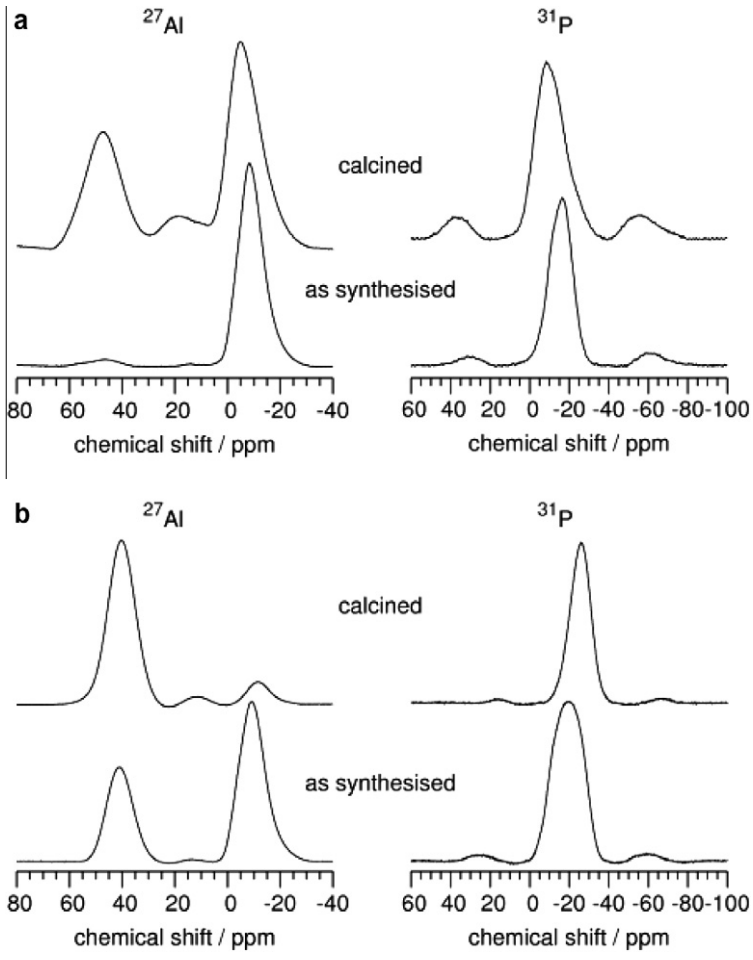

Fig. 6. ^{27}Al and ^{31}P MAS NMR spectra of as-prepared and calcined SAPO thin films (a) and xerogels (b).

that the calcined mesoporous SAPO xerogel contains much less framework defects than the calcined mesoporous SAPO thin film. The difference in the formation and in the response to thermal treatment between the two forms of SAPO material could stem from the effect of substrate and from the enhanced surface effects in case of thin film [16].

In microporous SAPOs ^{29}Si MAS NMR spectroscopy proved to be valuable tool that could provide information about the distribution of silicon within the material [28–31]. Most often either Si ↔ P or 2Si ↔ P + Al substitution was detected. The former mechanism can lead to isolated $Si(OAl)_4$ units or to aluminosilicate domains within SAPO. $Si(OAl)_4$ sites can generate weak acid sites. The latter substitution mechanism is often followed by additional substitution of three phosphorus atoms by silicon atoms, to avoid the formation of undesirable Si–O–P bonds [26]. Such a mechanism thus leads to formation of Si island or Si-rich domains within SAPOs and to appearance of $Si(OSi)_{4-n}(OAl)_n$ sites. While $Si(OSi)_4$ sites centered in the middle of Si island are neutral, Si sites at the border of Si islands, i.e. sites with $n > 0$, can give rise to moderate acid sites.

Because of low sensitivity of ^{29}Si nuclei, modest fraction of silicon in the sample, and small amount of the sample, we were not able to detect ^{29}Si MAS NMR spectra of SAPO films. However, we were able to record silicon spectra of xerogels and they are shown in Fig. 7. Although the signals in the spectra of the as-prepared xerogels are weak, one can identify at least three different silicon contributions. The analysis can be more reliably performed on the spectra of the calcined xerogel. ^{29}Si MAS and ^{1}H–^{29}Si CPMAS spectra can be roughly decomposed into four resonances with chemical shifts of −91, −100, −107, and −113 ppm. The resonances at −107 and −113 ppm belong to $Si(OSi)_3(OAl)$ and $Si(OSi)_4$ units [28–31], respectively. Their intensities are large in the ^{29}Si MAS spectrum and are not enhanced by cross polarization from protons. The resonances at −91 and −100 ppm could, consequently, be assigned to $Si(OSi)_2(OAl)_2$, $Si(OSi)(OAl)_3$ or $Si(OAl)_4$ units. However, the two resonances are substantially enhanced by cross polarization, which suggests that instead of one or two OAl or OSi groups, these silicon sites could bear one or two terminal OH groups. A reliable assignment of these two resonances is thus not possible and we cannot be sure whether there are or there are not $Si(OAl)_4$ units present in the mesoporous SAPO. Nevertheless, the intensity of the unassigned resonance at −91 ppm is much smaller than are the intensities of $Si(OSi)_{4-n}(OAl)_n$ units with $n < 4$, showing that silicon predominantly forms Si-rich domains within the mesoporous SAPO xerogel.

Incorporation of paramagnetic Mn ions into the silico-aluminophosphate material drastically increases spin–lattice relaxation rate for all NMR-active nuclei of the sample. It also results in broadening of NMR signals and in appearance of intense spinning sidebands. The spectra of ^{27}Al and ^{31}P nuclei (Fig. 8) suggest that mesoporous frameworks of MnSAPO films contain more defect sites and are substantially less condensed than the frameworks of manganese-containing xerogels. The accelerated spin–lattice relaxation allowed us to reduce repetition delay in silicon spectroscopy of MnSAPO samples by two orders of magnitude and therefore to obtain acceptable ^{29}Si MAS NMR spectra as quickly as in few hours (see Fig. 9). The spectra of the as-prepared and calcined

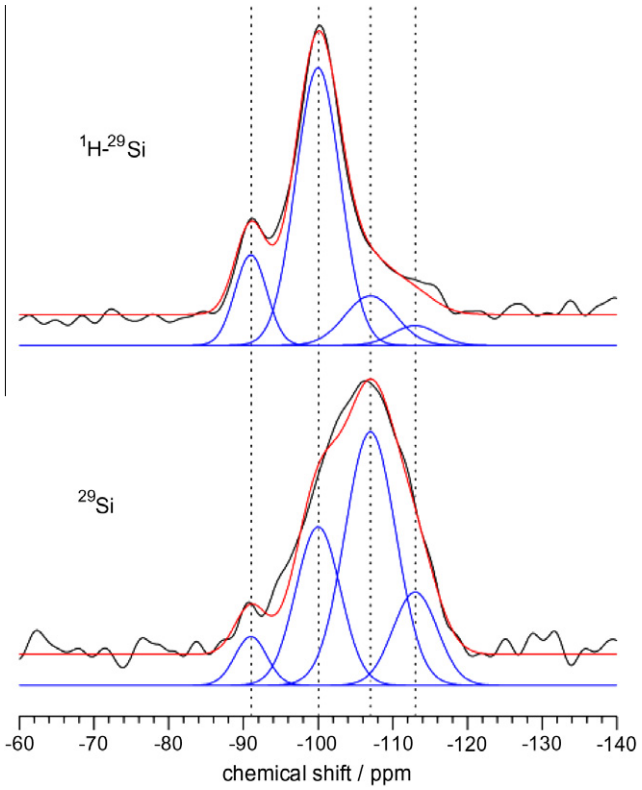

Fig. 7. ^{29}Si MAS (bottom) and ^{1}H–^{29}Si CPMAS (top) NMR spectra of the as-prepared and calcined SAPO xerogels. (Signal-to-noise ratio of the measurement was enhanced by CPMG detection. Echos of the time-domain signals had been co-added, so that Fourier transformation lead to enhanced and smooth spectra.) Rough decomposition of NMR spectra into individual contributions was performed (black line – measurement, red line – sum of contributions, blue line – individual contributions). Dotted vertical lines mark peak positions at −91, −100, −107, and −113 ppm. (For interpretation of the references to colour in this figure legend, the reader is referred to the web version of this article.)

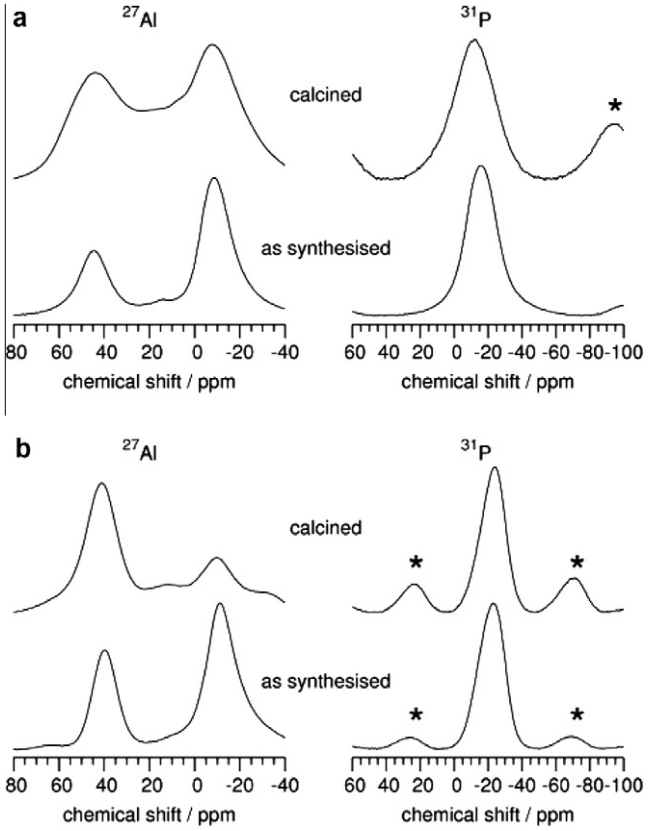

Fig. 8. ^{27}Al and ^{31}P MAS MAS NMR spectra of as-prepared and calcined MnSAPO thin films (a) and of as-prepared and calcined MnSAPO xerogels (b). Asterisk mark spinning sidebands.

MnSAPO xerogels are quite similar one to another and also to the spectrum of the calcined SAPO xerogel. The former two spectra both exhibit strong signals at −100 and −107 ppm. In comparison to them, silicon spectra of MnSAPO films exhibit much stronger contributions at −91 and −82 ppm. Taking into account that the framework of the film is poorly condensed, the two contributions could be assigned to $Si(OSi)_2(OH)_2$ and $Si(OSi)(OH)_3$ species, respectively. However, the spectra of MnSAPO thin films still exhibit signals at −107 and −113 ppm, which can again be assigned to $Si(OSi)_3(OAl)$ and $Si(OSi)_4$ units. Similarly as in SAPO xerogel, most probably silicon-rich domains are formed in MnSAPO thin film as well.

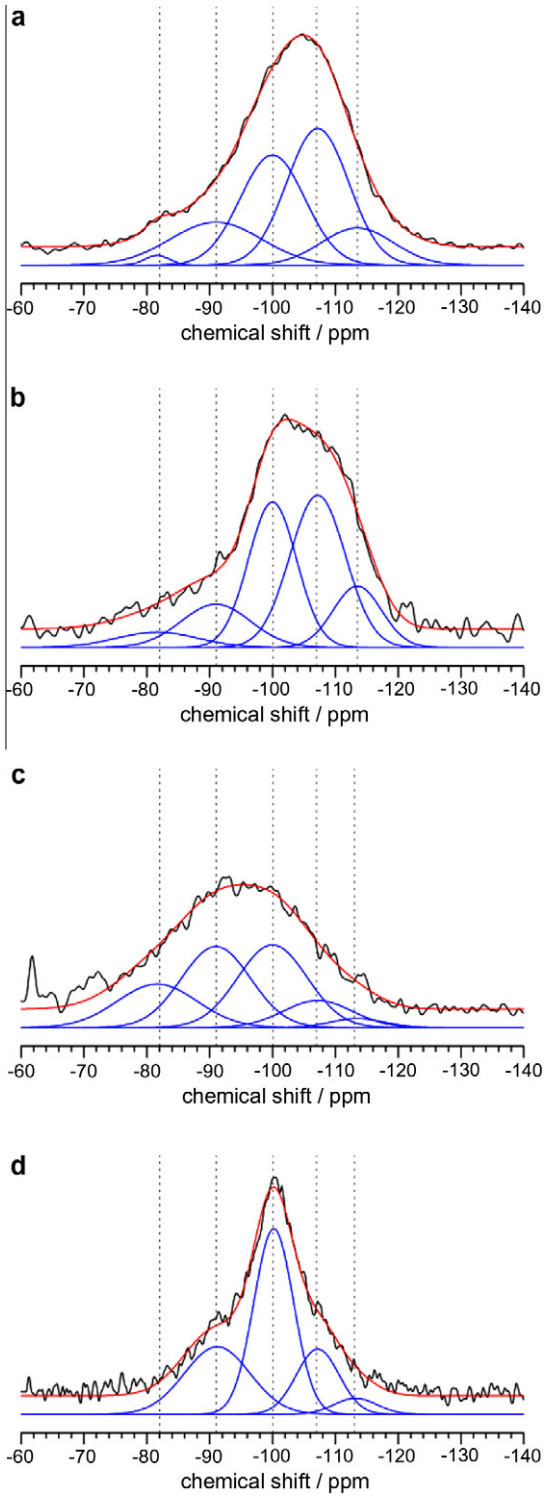

Fig. 9. Decpomposition of ^{29}Si MAS MAS NMR spectra of calcined (a) and as-prepared (b) MnSAPO xerogels and of calcined (c) and as-prepared (d) MnSAPO thin films.

Oxidation state and local environment of manganese was studied by X-ray absorption spectroscopy using XANES (X-ray Absorption Near Edge structure) and EXAFS (Extended X-ray Absorption Fine structure) methods. XANES identifies local symmetry and the average oxidation number of transition metal atoms by looking at the features present in the pre-edge and the edge regions. The average oxidation number of manganese cations in the Mn-containing samples was deduced from the energy shift of the manganese absorption edge [32,33]. The reference manganese samples with known manganese valence state and equal ligands (oxygen atoms) to manganese atoms as in the investigated samples were chosen. Based on XANES spectra of Mn metal, $Mn^{2+}O$, $K_3[Mn^{3+}(C_2O_4)_3]\cdot 3H_2O$ and $Mn^{4+}O_2$ a linear relation between the edge shift and the oxidation state was detected and the shift of 3.3 eV per oxidation state was determined. The observed shift is in agreement with previous observations [34,35].

Fig. 10 shows the normalized Mn XANES spectra of MnSAPO thin films and xerogels and of reference manganese compounds. The energy position of the Mn K-edge of all the MnSAPO samples is in the energy region between the Mn K-edge position of Mn^{2+} ($Mn^{2+}O$) and Mn^{3+} ($K_3[Mn^{3+}(C_2O_4)_3]\cdot 3H_2O$) reference compounds. Taking into account the above mentioned edge shift, we deduced that the average Mn valence states are 2.3 ± 0.05 (thus implying Mn^{3+}/Mn^{2+} = 30%/70%) for as-synthesized MnSAPO xerogel, 2.5 ± 0.05 (Mn^{3+}/Mn^{2+} = 50%/50%) for calcined MnSAPO xerogel, 2.35 ± 0.05 (Mn^{3+}/Mn^{2+} = 35%/65%) for as-synthesized MnSAPO thin film, and 2.4 ± 0.05 (Mn^{3+}/Mn^{2+} = 40%/60%) for calcined MnSAPO thin film. XANES thus shows that both Mn^{2+} and Mn^{3+} cations are present in as-synthesized and calcined MnSAPO xerogels and thin films. The amount of Mn^{3+} increases slightly upon calcination, in both xerogels and thin films. A slightly bigger amount of Mn^{3+} is present in calcined xerogels (50%) than in thin films (40%).

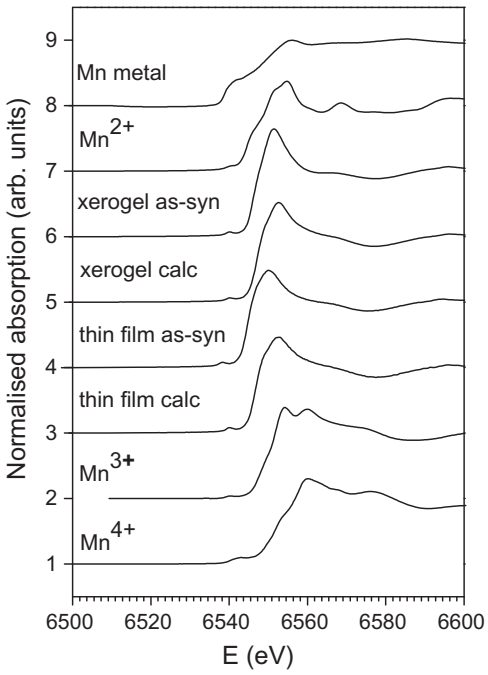

Fig. 10. Normalized Mn K-edge XANES spectra of as-synthesized and template-free MnSAPO xerogels and thin films and of Mn reference samples (Mn metal, $Mn^{2+}O$, $K_3[Mn^{3+}(C_2O_4)_3]\cdot 3H_2O$, and $Mn^{4+}O_2$). The spectra are displaced vertically for clarity. They were extracted by a standard procedure [32].

Table 1
Structural parameters of the nearest coordination shells around Mn atom in the as-synthesized and template-free MnSAPO: type of neighboring atom, average number N, distance R, and Debye–Waller factor σ^2. The amplitude reduction factor ($S_0^2 = 0.80 \pm 0.05$) was determined on MnO and kept fixed during the fit. Uncertainties in the last digit are given in the parentheses.

Neighbor	N	R (Å)	σ^2 (Å^2)
As-synthesized MnSAPO xerogel			
O	4.0(5)	2.27(1)	0.006(1)
Calcined MnSAPO xerogel			
O	0.6(2)	1.87(1)	0.010(1)
O	3.5(3)	2.15(1)	0.010(1)
As-synthesized MnSAPO thin film			
O	2.4(4)	2.10(2)	0.006(2)
O	2.4(4)	2.27(2)	0.006(2)
P	1	2.94(2)	0.010(2)
O	4	3.46(2)	0.020(5)
Calcined MnSAPO thin film			
O	0.5(3)	1.82(1)	0.007(1)
O	3.5(3)	2.07(1)	0.007(1)

The description of a short-range order around manganese atoms in terms of the number of neighbors, distances, and thermal and static disorder within the range of those distances was obtained by EXAFS. Results of quantitative analysis of Mn K-edge EXAFS spectra are presented in Table 1. Fourier transforms of k^3-weighted Mn EXAFS spectra of as-synthesized and calcined MnSAPO xerogels and thin films, together with best-fit EXAFS models, are shown in Fig. 11. Manganese cations of as-synthesized MnSAPO xerogel are coordinated to four oxygen atoms in the first coordination shell at a distance of 2.27 Å. Two shells of neighbors are found around manganese cations in the as-synthesized MnSAPO thin film. The quantitative EXAFS analysis shows that the first Mn coordination shell contains oxygen atoms, whereas the second shell consists of phosphorous and oxygen atoms. The atomic species of neighbors in consecutive shells were identified by their specific scattering factors and phase shifts. Manganese cations of as-synthesized MnSAPO thin film are also coordinated to four oxygen atoms in the first coordination shell, but two of them are at a shorter distance of 2.10 Å and two of them at a longer distance of 2.27 Å. Manganese cations within calcined MnSAPO xerogel and calcined MnSAPO thin film are coordinated to four oxygen atoms in the first coordination shell, again two of them are at shorter and two at longer. The short distances of 1.87 Å and 1.82 Å for MnSAPO xerogel and for MnSAPO thin film, respectively, are consistent with the average tetrahedral Mn^{3+}–O distance of 1.93(4) Å reported for $MnAsO_4$ [36]. There is no experimental indication for Mn atoms in the second coordination shell.

The results of XANES and EXAFS analyses on the calcined MnSAPO xerogels and thin films show that there are Mn^{3+} and Mn^{2+} cations present in the MnSAPO frameworks in almost equal amounts. In the calcined MnSAPO film and xerogel there are Mn cations coordinated to four oxygen atoms, indicating that Mn ions are located in tetrahedral environment. This suggests that manganese is incorporated into the aluminophosphate framework of the mesoporous materials. The four oxygen atoms are not all equally distant from manganese, implying that the MnO_4 tetrahedra are distorted.

4. Conclusions

Mesoporous SAPO and MnSAPO thin films have been synthesized via sol–gel procedure and successfully deposited on glass substrates via dip-coating in the presence of nonionic block copolymer surfactant Pluronic F127. Xerogels were prepared to compare two different ways of using the precursor solution. SAXS measurements showed that both thin films have highly ordered mesostructures, which exhibit body centered cubic symmetry. The cubic mesostructures of SAPO and MnSAPO thin films were confirmed also by TEM, SEM and AFM microscopies. AFM measurements further showed that the pores were well oriented in the planes parallel to the substrate, and that thin films were composed of domains, several hundred nanometers wide, which were arranged into a mosaic in the *xy* plane. The mesostructures remained stable up to at least 400 °C.

Incorporation of silicon and manganese into the aluminophosphate frameworks were studied by solid-state NMR and X-ray absorption spectroscopy. NMR spectra of xerogels showed that silicon is not homogeneously distributed throughout the farmework but it gatheres into silicon-rich domains. At the borders of such domains $Si(OSi)_3(OAl)$ units were detected. Such species could give rise to moderately acid catalytic sites. $Si(OSi)_3(OAl)$ units were detected also in MnSAPO thin films. NMR spectroscopy furthermore showed that the calcined mesoporous SAPO and MnSAPO xerogels

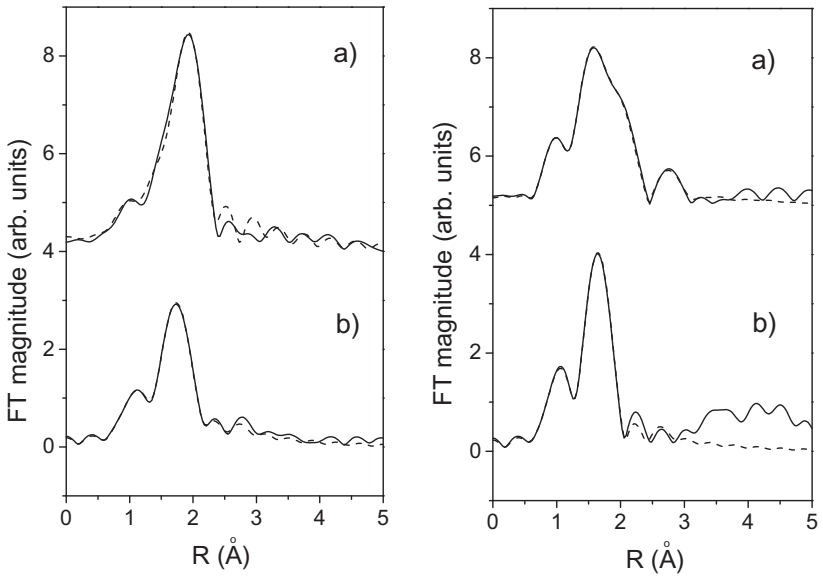

Fig. 11. Fourier transform magnitude of the k^3-weighted Mn EXAFS spectra of the (a) as-synthesized and (b) calcined MnSAPO xerogels, and of the (c) as-synthesized and (d) calcined MnSAPO thin films. (Solid line – experiment, dashed line – EXAFS model.)

contained much less framework defects than the calcined mesoporous SAPO and MnSAPO thin films. The difference in the formation and in the response to thermal treatment between the two forms of SAPO and MnSAPO materials could stem from the effect of substrate and from the enhanced surface effects in case of thin films. X-ray absorption spectroscopy showed that Mn^{3+} and Mn^{2+} cations are present in the MnSAPO frameworks in almost equal amounts. In calcined MnSAPO film and xerogel there are Mn cations coordinated to four oxygen atoms, which are not all equally distant from manganese. This indicates that Mn ions are located in distorted tetrahedra, which are most probably incorporated into aluminophosphate frameworks. Framework manganese ions can lead to catalytically active redox sites.

Acknowledgment

This work was supported by the Slovenian Research Agency research programs P1-0021, P1-0112, by DESY, the European Community under the FP6 Program "Structuring the European Research Area" contract RII3-CT-2004-506008 (IA-SFS) and ANPCyT (projects PICT 34518; PAE 2006 37063-00038). Access to synchrotron radiation facilities of HASYLAB and LNLS is acknowledged. We would like to thank Edmund Welter of HASYLAB for expert advice on beam line operation. Authors are indebted to Argentina-Slovenia project PA05E03 "Mixed mesoporous oxides" (SECyT-MHEST), and Ad Futura: Alejandra Calvo is gratefully acknowledged for her collaboration in sample preparation and SAXS measurements; Matjaž Mazaj is gratefully acknowledged for TEM measurements. GJAASI is a member of CONICET.

References

[1] J.S. Beck, J.C. Vartuli, W.J. Roth, M.E. Leonowicz, C.T. Kresge, K.D. Schmitt, C.T.-W. Chu, D.H. Olson, E.W. Sheppard, J.B. Higgins, J.L. Schlenker, J. Am. Chem. Soc. 114 (1992) 10834.
[2] C.T. Kresge, M.E. Leonowicz, W.J. Roth, J.C. Vartuli, J.S. Beck, Nature 359 (1992) 710.
[3] G.J.A.A. Soler-Illia, C. Sanchez, B. Lebeau, J. Patarin, Chem. Rev. 102 (2002) 4093.
[4] B. Kraushaar-Czarnetzki, W.H.J. Stork, R.J. Dogterom, Inorg. Chem. 32 (1993) 5029.
[5] B. Tian, X. Liu, B. Tu, C. Yu, J. Fan, L. Wang, S. Xie, G.D. Stucky, D.Y. Zhao, Nat. Mater. 2 (2003) 159.
[6] M. Tiemann, M. Froba, Chem. Mater. 13 (10) (2001) 3211.
[7] T. Kimura, Microporous Mesoporous Mater 77 (2005) 97.
[8] H.O. Pastore, S. Coluccia, L. Marchese, Annu. Rev. Mater. Res. 35 (2005) 351.
[9] N. Danilina, F. Krumeich, J.A. van Bokhoven, J. Catal. 272 (2010) 37.
[10] (a) M. Hartmann, L. Kevan, Chem. Rev. 99 (1999) 635;
(b) X.S. Zhao, G.Q. Lu, A.K. Whittaker, J. Drennan, H. Xu, Microporous Mesoporous Mater 55 (2002) 51.
[11] S. d'Arbonneau, A. Tuel, J. Auroux, Therm. Anal. Calorimetry 56 (1999) 287.
[12] T.D. Conesa, R. Mokaya, Z. Yang, R. Luque, J.M. Campelo, A.A. Romero, J. Catal. 252 (2007) 1.
[13] S.T. Wilson, Stud. Surf. Sci. Catal. 137 (2001) 229.
[14] A. Vieira, M.A. Tovar, C. Pfaff, P. Betancourt, B. Méndez, C.M. López, F.J. Machado, J. Goldwasser, M.M. Ramírez de Agudelo, M. Houalla, J. Molecular Catal. A: Chemical 144 (1999) 101.
[15] C. Sanchez, C. Boissiere, D. Grosso, C. Laberty, L. Nicole, Chem. Mater. 20 (2008) 682.
[16] M. Mazaj, S. Costacurta, N. Zabukovec Logar, G. Mali, N. Novak Tušar, P. Innocenzi, L. Malfatti, F. Thibault-Starzyk, H. Amenitsch, V. Kaučič, G.J.A.A. Soler-Illia, Langmuir 24 (12) (2008) 6220.
[17] D. Grosso, F. Cagnol, G.J.A.A. Soler-Illia, E.L. Crepaldi, H. Amenitsch, A. Brunet-Bruneau, A. Bourgeois, C. Sanchez, Adv. Funct. Mater. 14 (2004) 309.
[18] G.J.A.A. Soler-Illia, P. Innocenzi, Chem. Eur. J. 12 (2006) 4478.
[19] Z. Luan, D. Zhao, H. He, J. Klinowski, L. Kevan, J. Phys. Chem. B 102 (1998) 1250.
[20] N. Zabukovec Logar, N. Novak Tušar, G. Mali, M. Mazaj, I. Arčon, D. Arčon, A. Rečnik, A. Ristić, V. Kaučič, Microporous Mesoporous Mater 96 (2006) 386.
[21] N. Zabukovec Logar, N. Novak Tušar, A. Ristić, G. Mali, M. Mazaj, V. Kaučič, in: V. Valtchev, S. Mintova, M. Tsapatsis (Eds.), Ordered Porous Solids: Recent Advances and Prospects, Elsevier, Amsterdam, 2009, pp. 101–126.
[22] J.W. Wiench, V.S.-Y. Lin, M. Pruski, J. Magn. Reson. 193 (2008) 233.
[23] J.J. Rehr, R.C. Albers, S.I. Zabinsky, Phys. Rev. Lett. 69 (1992) 3397.
[24] B. Ravel, M. Newville, J. Synchrotron Rad. 12 (2005) 537.
[25] (a) G.J.A.A. Soler-Illia, E.L. Crepaldi, D. Grosso, D. Durand, C. Sanchez, Chem. Commun. (2002) 2298;
(b) E.L. Crepaldi, G.J.A.A. Soler-Illia, D. Grosso, F. Ribot, F. Cagnol, C. Sanchez, J. Am. Chem. Soc. 125 (2003) 9770;
(c) P. Innocenzi, P. Falcaro, D. Grosso, F. Babonneau, J. Phys. Chem. B 107 (2003) 4711.
[26] M.P. Tate, V.N. Urade, J.D. Kowalski, T.-C. Wei, B.D. Hamilton, B.W. Eggiman, H.W. Hillhouse, J. Phys. Chem. B 110 (2006) 9882.
[27] P.C. Angelomé, G.J.de.A.A. Soler-Illia, Chem. Mater. 17 (2005) 322.
[28] C.S. Blackwell, R.L. Patton, J. Phys. Chem. 92 (13) (1988) 3965.
[29] J.A. Martens, P.J. Grobet, P.A. Jacobs, J. Catal. 126 (1) (1990) 299.
[30] J. Chen, P.A. Wright, J.M. Thomas, S. Natarajan, L. Marchese, S.M. Bradley, G. Sankar, C.R.A. Catlow, P.L. Gai-Boyes, R.P. Townsend, C.M. Lok, J. Phys. Chem. 98 (40) (1994) 10216.
[31] R. Vomscheid, M. Briend, M.J. Peltre, P.P. Man, D. Barthomeuf, J. Phys. Chem. 98 (38) (1994) 9614.
[32] J. Wong, F.W. Lytle, R.P. Messmer, D.H. Maylotte, Phys. Rev. B 30 (1984) 5596.
[33] I. Arčon, B. Mirtič, A. Kodre, J. Am. Ceram. Soc. 81 (1998) 222.
[34] T. Ressler, J. Wong, J. Roos, J. Synchrotron Radiat. 6 (1999) 656.
[35] N. Novak Tušar, N. Zabukovec Logar, G. Vlaic, I. Arčon, D. Arčon, N. Daneu, V. Kaučič, Microporous Mesoporous Mater 82 (2005) 129.
[36] M.A.G. Aranda, J.-P. Attfield, S. Bruque, Inorg. Chem. 32 (1993) 1925.